Natural Hazards (2023) 116:3685–3702
https://doi.org/10.1007/s11069-023-05831-3

ORIGINAL PAPER

Failure behavior and mechanism of a slope under the action of earthquake after rainfall

Bing Yang[1] · **Jiangrong Hou**[1] · **Zihong Zhou**[1] · **Jincheng Gou**[1]

Received: 17 September 2021 / Accepted: 4 December 2022 / Published online: 30 January 2023

Abstract
Earthquake and rainfall may be coupled, which will lead to landslides easily, but the studies about this problem are at the initial stage. In this paper, the failure behavior and mechanism of a slope under the action of earthquake after rainfall were investigated with a shaking table test, based on similarity law. The experimental results showed that the failure process of the slope during earthquake after rainfall undergoes four characteristic stages. There exist velocity zoning in the slope during failure. The moisture content of soil in the slope has different growth rates at different positions during rainfall. Transient and cumulative pore water pressure occurs in the slope during earthquake after rainfall. However, due to the short period of earthquake action, the soil moisture content is not very sensitive to this action, but the pore water pressure changes sharply during earthquake. Under the combined action of rainfall and earthquake, there is a multi-physical field effect in the slope. Rainfall weakens the strength of the soil, mainly causes local instability of the slope. More extensive damage of the slope is caused under the combined action of seismic inertia force.

Keywords Failure behavior · Failure mechanism · Earthquake-rainfall coupling · Shaking table test

1 Introduction

Slope is widely distributed in the world, and its stability has been extensively concerned (Lin et al. 2006; Chen et al. 2013; Taylor, 1937; Yang et al. 2016, 2019; Srilatha et al. 2013; Chang et al., 2021). Rainfall and earthquakes are the main two common triggering factors that induce landslides (Wang et al. 2019; Chang et al., 2021; Song et al., 2021). The failure process, failure mechanism and related dynamic responses of slope induced by rainfall and earthquake are the focuses of research (Wang and Sassa 2003; Tohari et al. 2007; Lin et al. 2009; Lu et al., 2012a, 2012b; Chang et al. 2021).

Existent studies have shown that shallow soil landslides are more common in rainfall-induced landslides (Zhang et al. 2011; Lu et al., 2012a, 2012b), and most of the deep landslides induced are accumulation landslides influenced by bedrock interface. Some scholars

✉ Bing Yang
Yangb@home.swjtu.edu.cn

[1] School of Civil Engineering, Southwest Jiaotong University, Chengdu 610031, China

have studied various failure characteristics of slope in rainfall through laboratory tests (Wang and Sassa 2003; Tohari et al. 2007; Lin et al. 2009; Wu et al. 2017). The results show that the time of the initial landslide mainly depends on the degree of saturation of the soil near the toe of the slope. If the soil near the toe of the slope is close to saturation, no matter whether the other parts are saturated or not, the soil slope will always be in failure (Tohari et al. 2007). In addition, the moisture content in the failure area is close to saturation, but most of the soil in the unstable slope is still in an unsaturated state (Wang and Sassa 2003). Furthermore, high-intensity rainfall is easy to cause flowslide failure and erosion of the slope, while the rainfall with low intensity and long duration is easy to increase the pore water pressure of the deep soil of the slope, and the scale of the landslide is also larger (Tohari et al. 2007). Previous studies have shown that high pore water pressure is produced in the process of slope failure (Wang and Sassa 2003; Moriwaki et al. 2004).

The failure process and characteristics of slope under earthquake can make people intuitively study the characteristics and possible harm of slope failure and provide a basis for slope stability analysis. Laboratory tests showed that under the action of strong earthquake, the main deformation mode of clay slope is deep rotation / translation slip, and the deformation is mainly concentrated along one or more shear planes (Wartman et al. 2005; Yang et al. 2018). The soil moisture content has a great influence on the earthquake-induced slope failure mode (Yang et al. 2018, 2019). The slope with low moisture content mainly shows the shock crack-collapse (dispersion) failure mode, while the slope with high moisture content mainly shows the shock crack-creep failure behavior (Yang et al. 2018). It is also found that the characteristics of the bedrock interface below the slope have an obvious influence on the instability mode of the slope (Yang et al. 2018). The results reported by Du and Lu (2011) have shown that if the slope contains a certain composition of liquefied soil, this part of the soil may produce liquefaction under the action of earthquake, which may lead to slope failure. It is believed that earthquakes have two effects on slopes, i.e., the action of seismic inertia force and the increase and accumulation of excess pore water pressure induced by earthquake (Yang et al. 2018). For slopes with different soil properties, these two effects are different.

In some cases, earthquakes and rainfall may interact with each other and produce coupling effects, which will easily lead to landslides. For instance, a large earthquake with a moment M7.6 struck Padang Province, West Sumatra, Indonesia, in 2009, triggering landslides in Tandikat, Padang Pariaman Regency. The landslides occurred during rainfall, and originated on mountains mantled with loose pumice (Faris and Wang 2014). In 2013, a M6.6 earthquake occurred in Minzhang after 20 days of consecutive rainfall, Gansu Province, which led to landslides (Wang et al. 2021). At this condition, there will have some new changes in the failure characteristics and mechanism of slope. This problem has attracted interests of some researchers (Chang et al. 2007; Faris and Wang 2014; Wang et al. 2017; Chen et al. 2020; Martino et al. 2020). Chang et al. (2007) investigated the effect of earthquake after rainfall on the landslides using logistic regression. The initiation mechanism of an earthquake-induced landslide during rainfall has been investigated based on the variation of pore water pressure (Faris and Wang 2014). Large-scale shaking table tests have been performed to study the failure mechanism and dynamic response of loess slope under the coupling action of rainfall and earthquakes (Wang et al. 2017). The influence of duration of time between rainfall and earthquake on the failure mode and dynamic characteristics of low-angle loess slope has been investigated (Chen et al. 2020). Martino et al. (2020) analyzed the mechanism of landslides induced by the Morisse earthquake in Italy (M_W5.1), and their results showed that rainfall increases soil saturation, and then landslides occur under the action of seismic forces. So far, the failure mechanism of a slope

under the action of earthquake after rainfall (coupling effect between them) has not been revealed clearly due to limited investigation.

At present, the failure of the homogeneous loess slope has been studied by some researchers. However, there is a great difference in characteristics between loess and non-loess soil. Non-loess slopes account for most of the world. For the study on dynamic responses of non-loess slopes under earthquake after rainfall, it is still at the initial stage, and the failure mode and failure mechanism of the slope need to be further investigated. In this study, the gravel soil slope with bedrock was selected as the target slope.

The aim of this paper is to explore the failure behavior and failure mechanism of gravel soil slope with bedrock under the action of earthquake after rainfall (see Fig. 2). The failure process and behavior of slope would be investigated in detail. The physical mechanism of slope failure would be analyzed. The typical slope in the rich rainfall area located in the seismic zone is selected as the geological prototype. The model slope was constructed using similar materials prepared according to the law of similarity. The acceleration sensors, pore water pressure sensors, moisture content sensors and particle image velocimetry (PIV) were adopted to measure the dynamic response of the slope in the test to investigate the failure mechanism of slope. A HD camera was used to record the failure process during the test. Through analyzing the physical process of slope failure recorded by PIV and HD camera, the failure mode and failure characteristic of slope can be obtained.

2 Experimental details

2.1 Geological prototype

The eastern Himalayan tectonic junction in southeastern Tibet is one of the fastest uplifting areas of the Qinghai-Tibet Plateau. The complex geological environment determines the complexity of engineering geological problems in this area and gives birth to more landslides. The study area as a whole is located on the west side of the eastern Himalayan tectonic knot, and the canyon area in the first-order watershed between the Gangdise Mountains in the northwest and the Himalayas in the south, which belongs to the Lhasa block structurally and is located in the Dongjiu-Milin ductile shear zone. According to the different fault properties of different sections, it can be further subdivided into Lulang-Dongjiu left strike-slip shear zone, Dongjiu-Pailong ductile thrust shear zone and Tongdeng-Tongmai left strike-slip fault. The main exposed bedrock are Nianqintangula group gneiss, Yarlung Zangbo ophiolitic complex and a small amount of Neogene biotite monzonitic granite (Fig. 1). Quaternary loose deposits are mainly distributed on the surface of slopes and river valleys, and most of them are slope deposits, alluvial deposits and glacial deposits. Geomorphologically, the study area belongs to alpine canyon landform, and the whole is a "V" shape.

The main research area in this work is located in Lulang-Dongjiu section. The bedrock in this area is mainly biotite plagioclase gneiss and Yarlung Zangbo ophiolitic complex. Gneisses are developed in the rock mass, and the slopes on both sides of the valleys are 25°–35°. The high and steep quaternary loose deposits facing rivers and highways have formed high and steep slopes due to river cutting slopes and artificial excavation, and the material composition is block gravel soil with poor stability (Fig. 2). Soil landslides are mainly developed in this section. Earthquakes occur

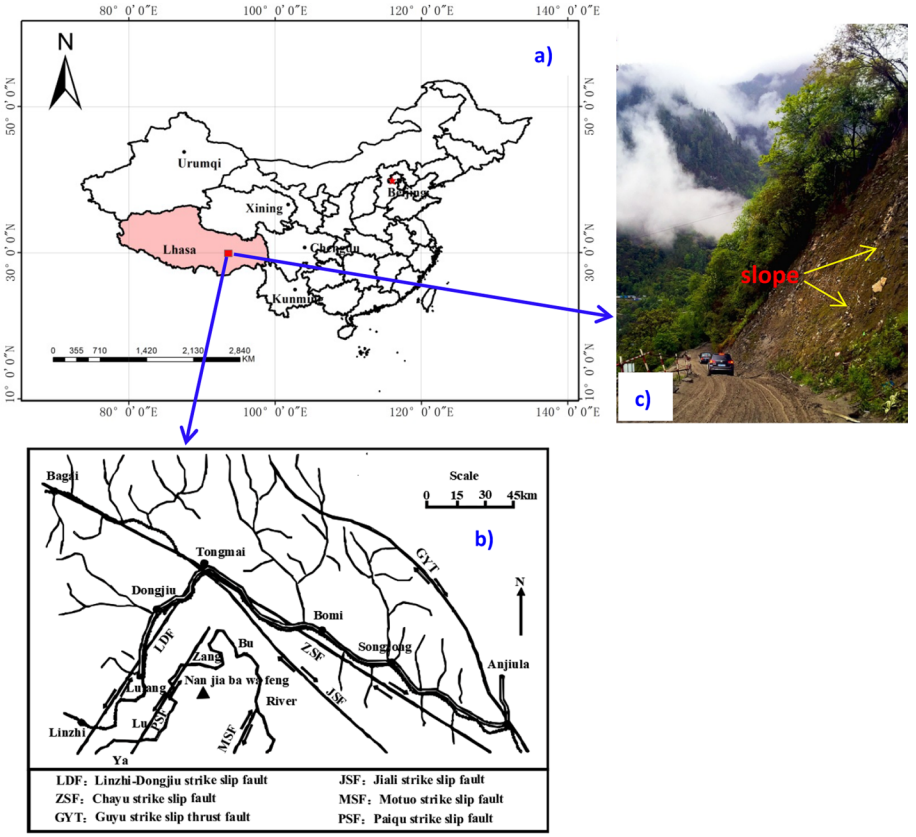

Fig. 1 **a** Location of study area, **b** geological structure of the eastern Himalayan tectonic junction, **c** the slope in prototype

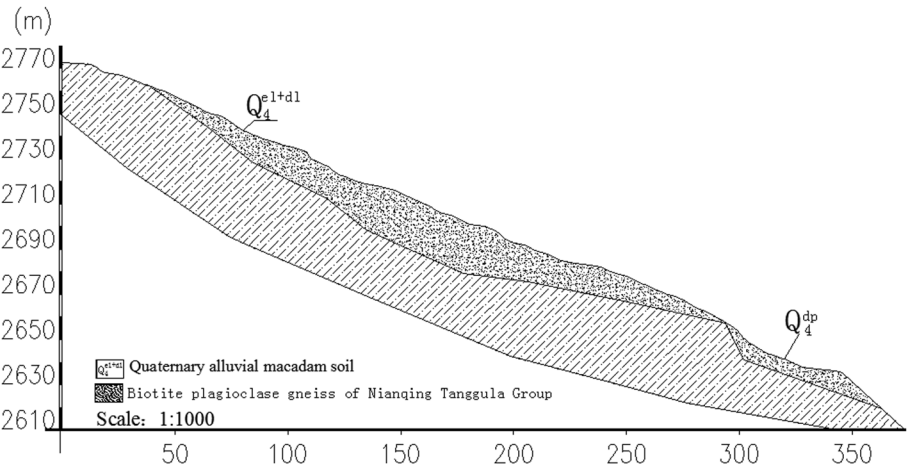

Fig. 2 Geological profile of a slope in prototype

Table 1 Physical and mechanical properties of soil from the prototype

Parameter	Value	Parameter	Value
Unit weight γ (kN/m^3)	14.2–16.9	Compressive modulus $E_{s1\text{-}2}$(MPa)	68–85
Natural moisture content w (%)	5.2–12.6	Poisson's ratio ν	0.27–0.28
Cohesion c (kPa)	21.3–37.8	Hydraulic conductivity k (cm/s)	$2.7–3.3\times10^{-4}$
Internal friction angle φ(°)	26–32	Liquid limit I_L (%)	25.1–28.3
		Plastic limit I_p (%)	17.3–18.1

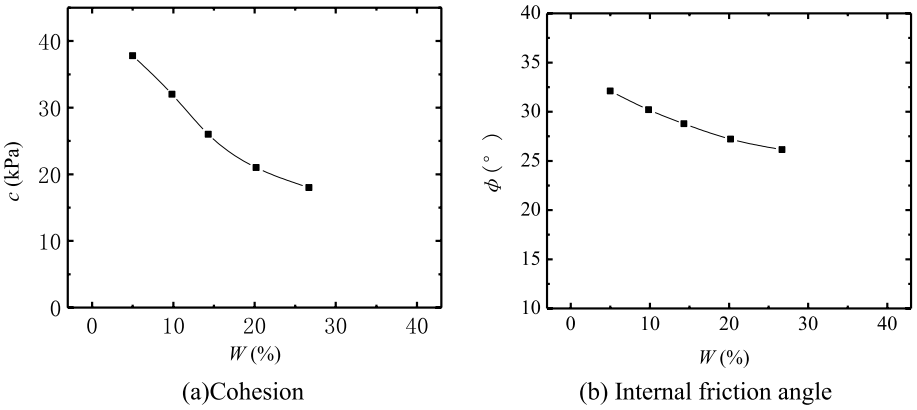

Fig. 3 Cohesion and internal friction angle of soil in prototype versus moisture content

frequently in this area, and the annual rainfall is abundant. The probability of landslide induced by rainfall and earthquake is very high.

In order to obtain the physical and mechanical properties of the soil in the prototype, the original soil sampler was used to take the soil sample from the field slope. The sample soil was put in a sealed plastic bag to ensure that the soil moisture is not lost in the process of transportation. Then, we bring it back to the laboratory for geotechnical tests with various parameters. Sieving test showed that the composition of soil in the prototype includes 13.3% of crushed stone, 82.6% of clay and 4.1% of silt. Laboratory tests including direct shear test and triaxial test were conducted using disturbed specimen. The physical and mechanical parameters of soil are listed in Table 1. It is indicated from Table 1 that the soil has certain cohesion and larger internal friction angle. The unit weight of soil in prototype listed in Table 1 indicates that the soil is at the relatively loose state.

The rainfall will significantly affect the shear strength of the soil. The relationship between the shear strength parameter and the moisture content were investigated, as plotted in Fig. 3. The results shown in the figure indicate that the cohesion and internal friction angle of soil decrease progressively with the moisture content, which means that the rainfall will lead to the decrease in shear strength of soil.

2.2 Test apparatus

An electromagnetic shaking table with a loading platform of 1.2 m × 1.2 m was used to exert earthquake load on the slope, which can simulate single-degree-of-freedom vibration of different waveforms. The shaking table has a payload of 1t and a displacement amplitude of ±51 mm. It can generate acceleration of 0.05–98 g with a frequency range of 2–3000 Hz. A test box with an adjustable bottom plate was designed to simulate the slope with bedrock interface below it, as shown in Fig. 4. The box is 1.8 m long, 0.32 m wide and 1.2 m high. The side wall of the box is transparent in order to record the process of slope failure with a high-precision camera.

2.3 Model slope in test

In the test, the model scale of slope height is set to $c_H = H_P/H_m = 266$ (where H_P is the height of the prototype, and H_m is the height of the model slope), which is the geometrical scale of similarity. The model scales of unit weight of soil and gravitational acceleration are set to $c_\gamma = 1$ and $c_g = 1$, respectively. The slope height H, unit weight γ and gravity acceleration g were selected as the fundamental parameters. Therefore, the similarity scales of other physical variables can be deduced according to similarity law, and the corresponding model law is listed in Table 2.

The model slope in this study has a height of 0.6 m, a length of 0.9 m, and a width of 0.32 m. The angles of bedrock interface below the overlying soil layer are set to $\theta_1 = 14°$ and $\theta_2 = 52°$, respectively. The slope angle in the test is 44°. Through direct shear test, the physical and mechanical properties of model materials were determined. The composition of the model materials consists of sand, barite powder, slag powder

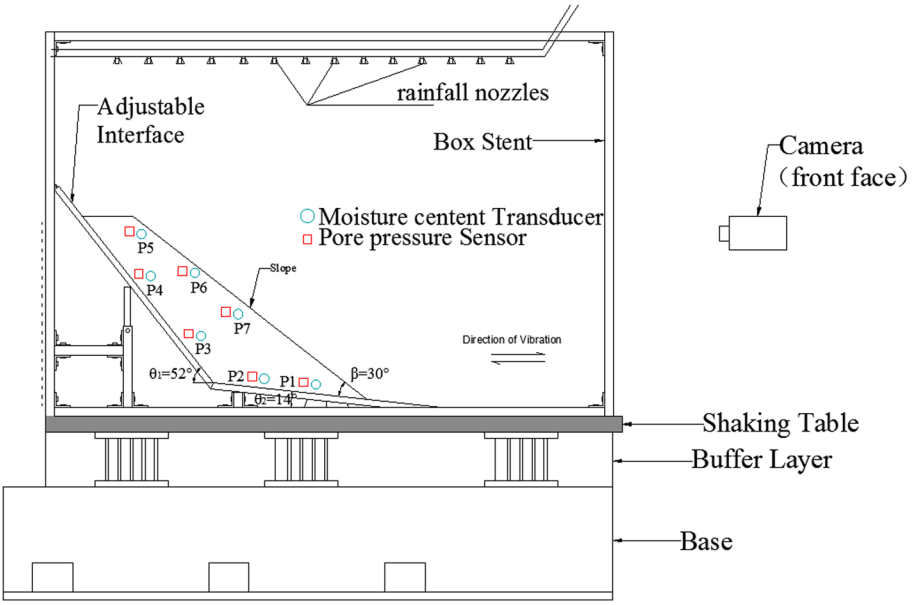

Fig. 4 Schematic of experimental setup

Table 2 Model law in the test

Parameter	Symbol	Similarity rule	Similar relation
Slope height	H	–	$c_H = 266$
Unit weight of soil	γ	–	$c_\gamma = 1$
Gravitational acceleration	g	–	$c_g = 1$
Slope angle	α	α	1
Upper interface inclination	θ_1	θ_1	1
Lower interface inclination	θ_2	θ_2	1
Cohesion	c	$c/\gamma H$	$c_c = c_\gamma c_H = 266$
Internal friction angle	$\emptyset$	$\emptyset$	1
Modulus of compressibility	E_s	$E_s/\gamma H$	$c_{Es} = c_\gamma c_H = 266$
Poisson's ratio	ν	ν	1
Moisture content	w	w	1
Permeability coefficient	k	$k/\sqrt{gH}$	$c_k = c_g^{0.5} c_H^{0.5} = 16$
Rainfall intensity	q	q/k	$c_q = c_k = c_g^{0.5} c_H^{0.5} = 16$
Rainfall duration	t_1	$t_1\sqrt{g/H}$	$c_{t_1} = c_g^{0.5} c_H^{-0.5} = 0.0625$
Principle vibration frequency	f	$f\sqrt{H/g}$	$c_f = c_H^{-0.5} c_g^{0.5} = 0.0625$
Peak acceleration of load	a	a/g	$c_a = c_g = 1$
Earthquake of duration	t_2	$t_s f$	$c_{ts} = c_H^{0.5} c_g^{-0.5} = 16$

and clay. The physical and mechanical parameters of the model materials at the initial stage are listed in Table 3. Several physical variables did not exactly match the similarity law, and other parameters had met it.

The method of layer construction was used to construct the slope model, and each layer was 10 cm. During the construction, the soil was rolled and compacted with a constant external force in order to keep the same porosity within the slope (Yang et al. 2018). White sand exhibiting a vertical banding distribution was set along the inner side of glass wall (Yang et al. 2018), so that the deformation of the slope could be observed.

2.4 Rainfall device

A rainfall simulator was self-designed. The simulator, which can spray water at intensities of 5–60 mm/h, possesses four nozzles at a height of 1.0 m above the bottom of the box. In the test, a constant intensity of 24 mm/h was implemented.

Table 3 Physical and mechanical properties of model materials at the initial stage

Parameter	Value	Parameter	Value
Unit weight, γ (kN/m^3)	15.5	Compressive modulus, E_{s1-2} (MPa)	8
Cohesion, c (kPa)	1.3	Poisson's ratio, ν	0.27
Internal friction angle, φ(°)	28	Hydraulic conductivity, k (cm/s)	1.3×10^{-4}

2.5 Instrumentation

A particle image velocimetry (PIV) was employed to measure the motion of soil particles within the slope. The size of the area tested was 600 mm × 400 mm, and the range of speed measurement is 0–2 m/s. The high-speed camera had a resolution of 2048 × 2048 pixels with a sampling rate of 750 fps. A EC-5 moisture sensor (Decagon Company, United States) was used to monitor the moisture content of the soil. A charge-type pore water pressure sensor (Tester Company, China) with an accuracy of 10 Pa, and a measuring range of 0–10 kPa was used to monitor the pore water pressure. The cameras with a normal sampling rate of 25 fps used to record the experimental phenomena were also arranged. Figure 4 shows the measurement arrangement. A high-speed data acquisition device (USB-6255, National Instruments USA) was employed to collect the data.

2.6 Test program

In order to investigate the slope failure behavior under the action of earthquake after rainfall, three groups of tests were carried out, namely rainfall of 188 min, 310 min, and 464 min. The acceleration time history was selected from the Comprehensive observation and Research Station of Alpine Environment in Southeast Tibet, Lulang Town, Linzhi City (Southeast Tibet Station for short). The typical time series and Fourier spectrum of acceleration recorded in an earthquake are shown in Fig. 5. It is indicated from the figure that PGA = 0.45 g, and predominant frequency is at 6–12 Hz. In the test, on the basis of this, a series of loading waveforms are obtained by amplifying and reducing the vibration amplitude. When rainfall stopped, the earthquake wave was immediately exerted on the slope. The duration of the input waves was 20 s, with the amplitude of the loading waves increased at intervals of 0.1 g individually until the critical value at which the slope became unstable was arrived at.

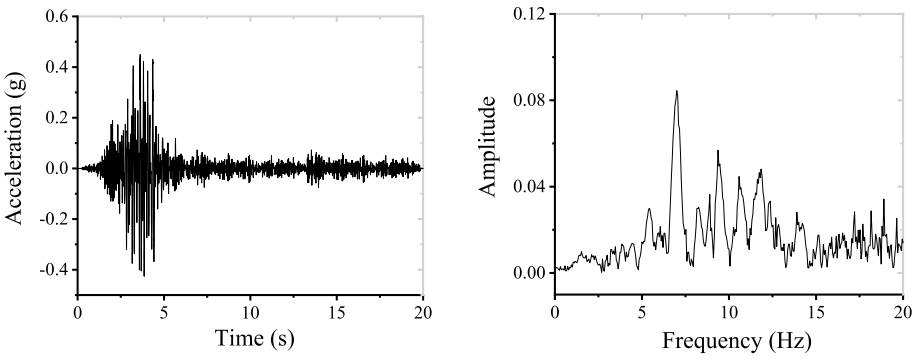

(a)Time history of acceleration (b) Fourier amplitude spectrum

Fig. 5 Time history of acceleration and Fourier amplitude spectrum (PGA = 0.45 g)

3 Failure process and behavior of slope

3.1 Failure process during rainfall

In this study, rainfall was acted on the slope firstly. Taking the rainfall duration of 310 min as an example, the typical results are plotted in Fig. 6. The failure process of the slope can be divided into three stages: failure initiation stage, failure expansion stage and foot failure stage. The first can be defined as failure initiation stage (see Fig. 6b). After 3 h and 34 min of rainfall, the soil is fluidized at the toe of the slope. The reason for this is that rain water gradually converges at the foot of the slope after it permeates into the slope, and the soil moisture content at the foot of the slope increases and the soil is softened progressively. The soil-fluidization phenomenon occurs under the combined action of rainfall erosion and internal seepage, which is the first stage, i.e., failure initiation stage. Then, it goes into the second stage, i.e., failure expansion stage. As the rain continues, the area of soil fluidization expands continuously (see Fig. 6c). This is the typically failure expansion stage. The third is foot failure stage. At this stage, after 5 h and 10 min of rainfall, the fluidization area of soil at the foot of the slope expands further, with a block-sliding failure occurring at the toe of the slope, as shown in Fig. 6d.

3.2 Failure process during earthquake after rainfall

When the rainfall stops, the earthquake load is exerted on the slope. The failure process of the slope during earthquake after rainfall is shown in Fig. 7. According to the tested results, the failure process can also be divided into four characteristic stages. When the Wenchuan earthquake wave with a peak acceleration of 0.577 g was exerted on the slope, there was no displacement in any part of the slope. In this case, it is defined as no deformation stage. However, when the peak acceleration of the Wenchuan earthquake wave was increased to 0.866 g, there was a small vertical displacement at the top of the slope. Moreover, there exhibits a slip surface along the interface between the soil and bedrock at the upper part of the slope, with the slope sliding slightly along the bedrock, as shown in Fig. 7c. This is called slight slip stage. When the input peak acceleration of the Wenchuan earthquake wave reached 1.010 g, the vertical displacement of the top of the slope increased further, with part of the soil from the middle of the slope to the toe of the slope deforming convexly, as

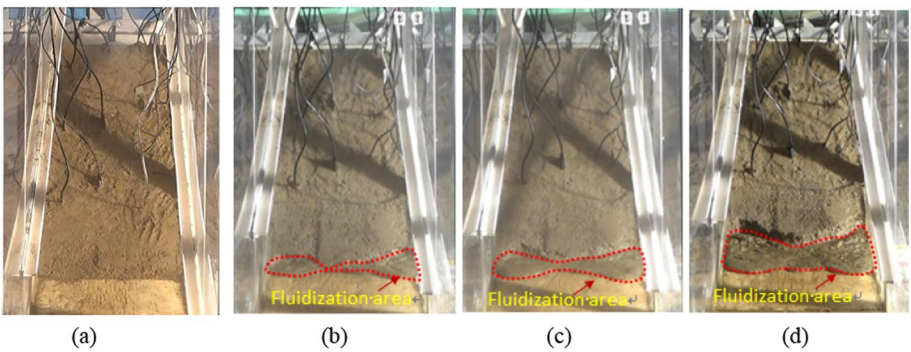

Fig. 6 Failure process of slope during rainfall. **a** Original state, **b** failure initiation stage, **c** failure expansion stage and **d** foot failure stage

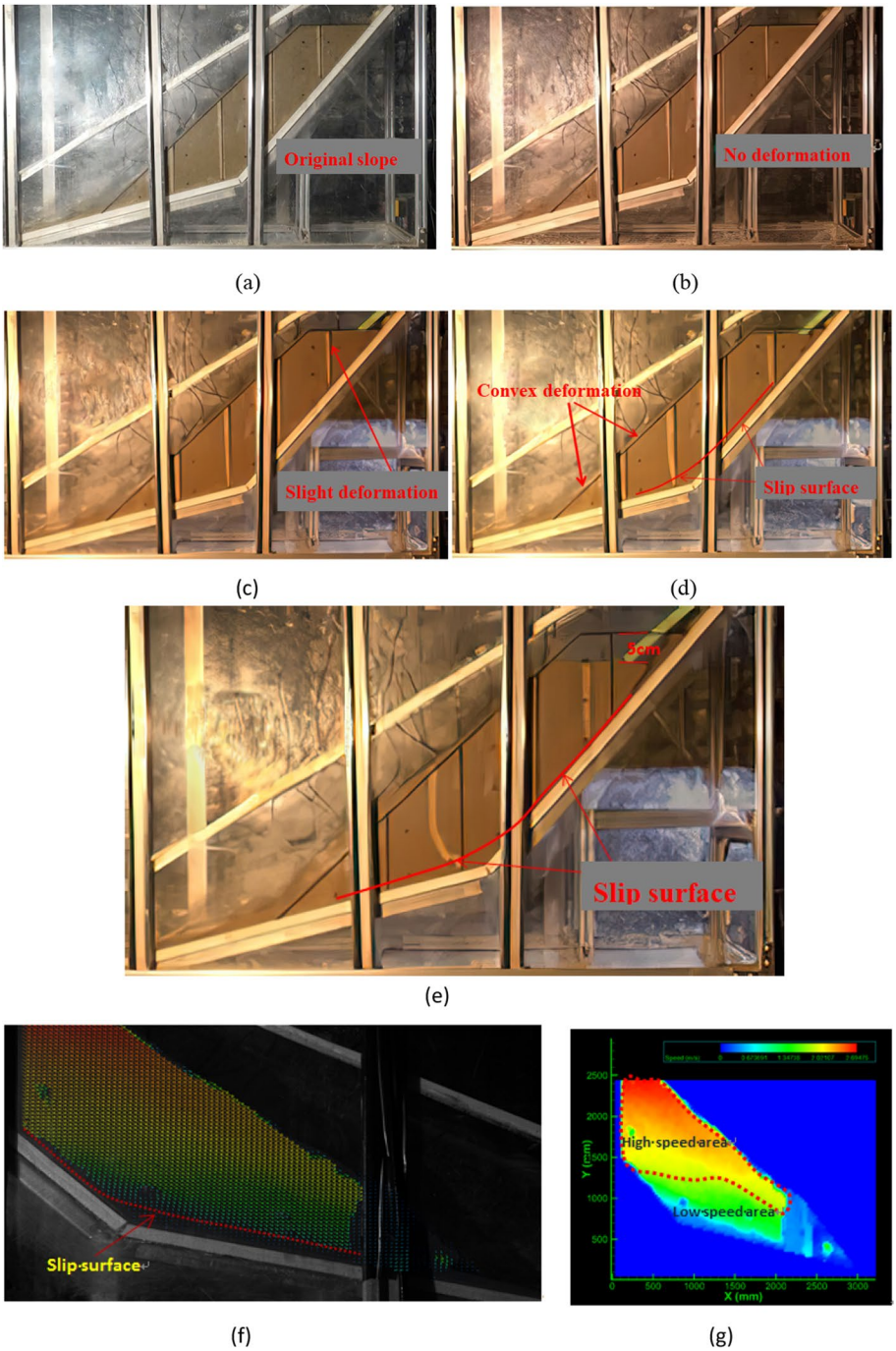

Fig. 7 Failure process of slope during earthquake after rainfall **a** original state, **b** no deformation stage (0.577 g), **c** slight slip stage (0.866 g), **d** slip initiation stage (1.010 g), **e** slope failure stage (1.443 g), **f** velocity vector of the soil particles at the time of failure (1.443 g) and **g** contour of velocity

can be seen from the deformation of the white line marked upon the slope. The upper soil of the slope slipped along the bedrock, whereas the lower soil slipped within the slope, as shown in Fig. 7d. This is called slip initiation stage. When the input peak acceleration of the Wenchuan earthquake wave was increased to 1.443 g, the slope deformation was enlarged further, with the vertical displacement at the top of the slope growing to 5 cm, and the convexity of the soil in the lower part of the slope becoming more acutely obvious, as shown in Fig. 7e, which is defined as slope failure stage.

During the failure process, the PIV system was used to record the motion of soil particle, and then the velocity of soil particle in the slope can be measured. From the velocity vector of the soil particles in the slope at the time of failure (Fig. 7f) and the velocity contour (Fig. 7g), it was found that there was a great difference of the velocity at different parts during the process of slope failure. The motion velocity is able to be divided into two obvious regions, namely the high-speed area located in the middle and upper part of the slope and the low-speed one in the middle and lower part. The velocity of soil particles on the lower side of the slope was close to zero, while the one at the top of the slope was the highest, reaching 2.69 m/s. If the earthquake continues, shear slip surfaces might potentially occur at the boundary between the two motion areas.

4 Failure mechanism of slope

4.1 Variation of moisture content

The moisture content of soil in slope is an essential parameter, which has a great influence on the strength of the soil. The variation in moisture volume content of the slope during 310 min of rainfall is plotted in Fig. 8. It can be seen from the figure that the moisture content of soil in the slope has different growth rates and stable values in different positions of the slope. The moisture content of the soil near the foot of the slope increases faster than that of the rest of the slope. Therefore, the strength of the soil in this region should decrease first and the failure initiation happened also first here. As shown in Fig. 8, the moisture content of the soil near the bedrock interface on the lower side of the slope was the highest, indicating that water converges at this location easily. Thus, the failure of slope occurred at the foot of the slope (Fig. 6), whereas the soil moisture content was the lowest

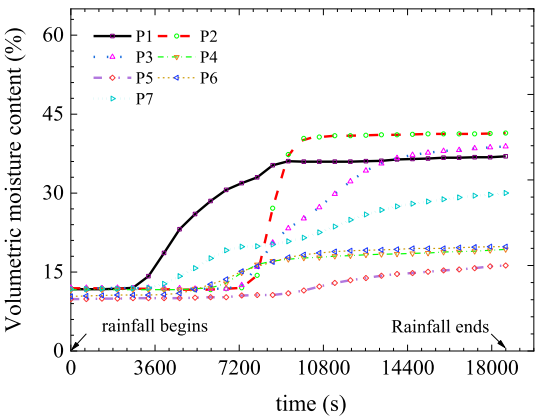

Fig. 8 Variation of volume moisture content of soil in slope during 140 min of rainfall

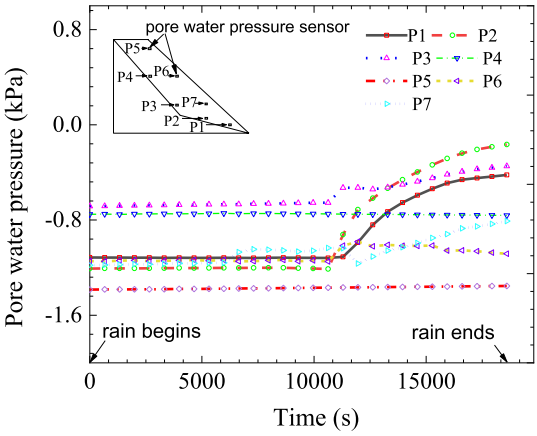

Fig. 9 Pore water pressure in slope during 310 min of rainfall

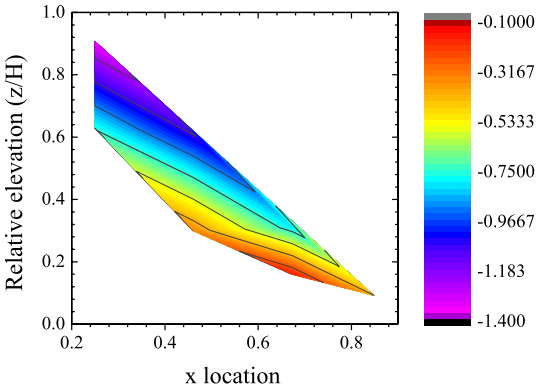

Fig. 10 Contour of pore water pressure in slope after 310 min of rainfall (unit: kPa)

near the upper part of the slope during the rainfall, indicating that rain water dissipates easily at that location. Therefore, the strength of soil at that area varies slowly and has a relatively high stability. During the earthquake, the variation of moisture content of the soil can nearly be neglected due to the very short period of vibration, so it is not analyzed here.

4.2 Variation of pore water pressure

4.2.1 Pore water pressure during rainfall

Pore water pressure reflects the stress state of soil. The higher pore water pressure corresponds to the lower effective stress of the soil. Therefore, the high pore water pressure may lead to slope failure under some conditions. The variation of pore water pressure within the slope during 310 min of rainfall is plotted in Figs. 9 and 10. It can be seen that during rainfall, the change of pore water pressure is consistent with the variation of moisture content. The pore water pressure within the middle and lower part of the slope, especially at the bottom of the slope, increased rapidly during rainfall, whereas that in the middle and upper parts of the slope, especially at the top of the slope, was basically unchanged. Therefore,

the effective stress of the soil near the foot of the slope decreases the most, compared with other location. Thus, the failure of slope first happened at the foot of the slope.

4.2.2 Pore water pressure during earthquake after rainfall

During earthquake, soil is subjected to periodic compression deformation, so the pore water pressure will also demonstrate periodic change. Figure 11 shows the variation of pore water pressure during seismic loading after rainfall. It shows from the figure that the peak value of pore water pressure increases with the intensity of seismic load, which indicates that the instantaneous strength of soil will decrease correspondingly. Therefore, the deformation of slope will increase with the earthquake load, as shown in Fig. 7.

For the same intensity of earthquake load, the pore water pressure at different locations within the slope undergoes different changes. There are two responses of pore water pressure during the action of earthquake: transient and cumulative pore water pressure. Figures 11 and 12 shows the variation of pore pressure during earthquake. The results indicate that the pore water pressure at the lower part of the slope near the bedrock interface (e.g., P1, P2) experienced transient change similar to the seismic waveform, which means that the peak value of pore water pressure changes almost synchronously with that of seismic load, and this is called the transient pore pressure response. From the pore water pressure responses of P1 and P2 (Fig. 12a, b), it can be seen that even after many times of vibration, the pore water pressure returned to its original level finally, indicating that there was almost no cumulative effect of pore water pressure. Figure 7e shows that there are nearly no deformation of soil at points P1 and P2, which is consistent with the variation in Fig. 12a, b. However, the pore water pressure (e.g., P3, P4) near the bedrock interface at the middle and upper parts of the slope presents not only transient response (Fig. 12a, b), but also shows cumulative response. When earthquake ceased, the pore water pressure was obviously higher than that prior to vibration, indicating that the soil has irrecoverable plastic deformation, which is also consistent with the fact that there are obvious displacements at P3 and P4 (Fig. 7e). For the soil at the upper part of the slope (e.g., at P5), there was nearly no change in pore water pressure during only rainfall (Fig. 9). The soil moisture content was also low (see Fig. 8), so the amplitude of transient pore pressure change was small during earthquake, and the cumulative pore pressure was not large, although the soil obviously

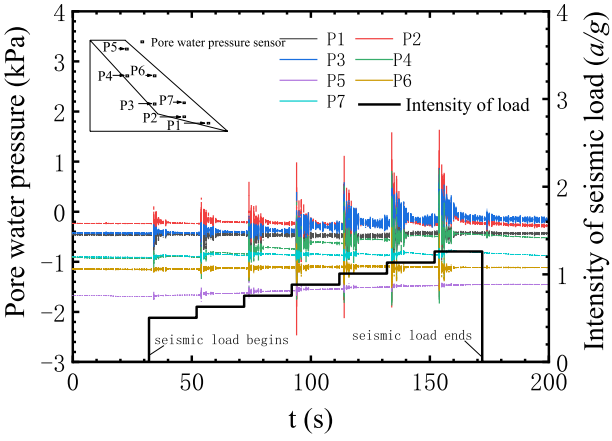

Fig. 11 Variation of pore water pressure versus time during seismic loading after rainfall

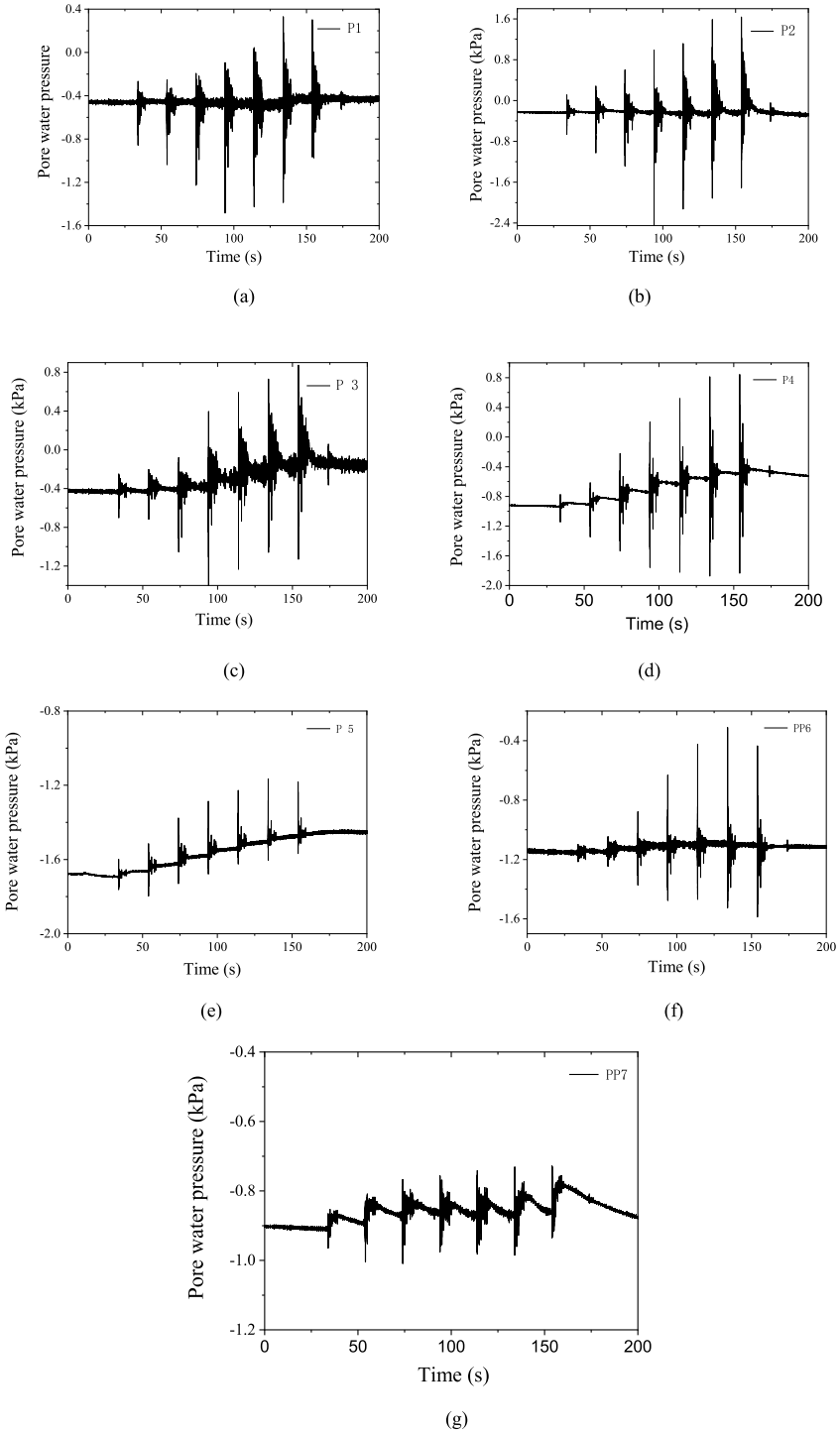

Fig. 12 Variation of pore water pressure at different points in slope during earthquake **a** at P1 point, **b** at P2 point, **c** at P3 point, **d** at P4 point, **e** at P5 point, **f** at P6 point, **g** at P7 point

displayed some plastic deformation during earthquake (see Fig. 12e). Near the middle and upper surfaces of the slope, the transient pore water pressure was small due to the low moisture content, and cumulative pore water pressure was basically nonexistent (e.g., at measuring point P6).

With respect to point P7 located within the middle and lower surface of the slope, the soil moisture content is in the middle level, whereas the transient pore water pressure also changed slightly. In addition, cumulative pore water pressure changed most obviously during vibration; however, this pressure dissipated quickly. The reason is that the soil at this location experienced plastic deformation, but the soil is relatively loose and the pores are large, so the rainwater moves outward quickly.

The above analysis indicates that the pore water pressure during earthquake is mainly controlled by soil deformation, and the influence of the pore water pressure on the deformation of soil is slight, compared with that of earthquake. Thus, it is indicated that the earthquake load is the key factor that leads to slope failure, and the pore water pressure induced by earthquake in the slope may not be the primary factor in some cases of combination of rainfall and earthquake.

5 Effect of rainfall duration on critical acceleration

In this section, the influence of rainfall duration on the critical acceleration of slope instability was discussed, and three groups of test results corresponding to 188 min, 310 min and 464 min of rainfall were analyzed. Figure 13 shows the relationship between the critical acceleration and rainfall duration. It can be seen from the figure that the critical acceleration corresponding to slope failure decreases almost linearly with the increasing rainfall duration, which means that the longer duration of the rainfall will greatly increase the risk of slope instability. It is also consistent with the conclusion of the variation of moisture content with time (Fig. 8).

6 Discussion

Rainfall will directly lead to the increase in soil moisture content and pore water pressure in the slope. However, the growth rate of moisture content is different in different positions of the slope, which has the characteristic of spatial distribution. Under the action of gravity,

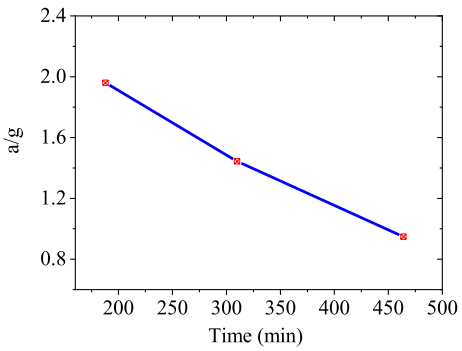

Fig. 13 Effect of rainfall time on critical acceleration of slope failure

rain water seeps downward and finally converges at the foot of the slope and flows out from the toe of slope, so the moisture content of the soil near the foot of the slope increases the fastest and is the first to reach saturation. With the continuous rainfall, the soil saturation area extends upward from the foot of the slope to the middle and top of the slope. Whether the soil in the middle and upper part of the slope can reach saturation depends on a variety of factors, including rainfall intensity, rainfall duration, soil permeability and so on. The change of pore water pressure is directly affected by soil moisture content, so it also has the characteristics of spatial distribution. Where the water content increases rapidly, the pore water pressure also increases quickly. However, under the action of earthquake, due to the short period of earthquake action, the soil moisture content is not very sensitive to this action. However, the pore water pressure changes sharply during the earthquake. The peak value of pore water pressure changes almost synchronously with that of seismic load, and this is called the transient pore pressure response. On the whole, there are two responses for the pore water pressure: transient response and cumulative response. The cumulative response characteristics of pore water pressure appear in the place where obvious plastic deformation of soil occurs in the slope. When the slope soil has only elastic deformation but no obvious plastic deformation, the pore water pressure is mainly transient response.

In addition, the strength of soil is also affected by moisture content. Where the moisture content increases quickly, the soil strength also decreases rapidly. Rain water is also easy to converge at the interface between the bedrock and covering layer, so the strength of the soil at that place decreases much faster. Therefore, the slope is easy to form a sliding surface at the bedrock interface.

Under the combined action of rainfall and earthquake, there is a multi-physical field effect in the slope, i.e., softening effect of soil induced by rain water, increasing effect of pore water pressure and dynamic effect induced by earthquake. Rainfall weakens the strength of the soil, mainly causes local instability of the slope. More extensive damage of the slope is caused under the combined action of seismic inertia force.

7 Conclusions

The failure behavior and mechanism of a slope under the action of earthquake after rainfall have been investigated with a shaking table test. Based on the results of test, the following conclusions can be drawn:

(1) The failure process of the slope under the action of rainfall can be divided into three stages: failure initiation stage, failure expansion stage and foot failure stage. The failure process of the slope during earthquake after rainfall has four characteristic stages: no deformation, slight slip, slip initiation and slope failure stages. In this study, the rainfall mainly leads to local failure of slope, but the earthquake after rainfall induces whole failure. The velocity of soil particles during the failure of the slope may have different values at different position. In this study, it can mainly be divided into two areas, namely the high-speed area and the low-speed one. The sliding surface mainly occurs at the interface between the two areas.

(2) Rainfall will directly lead to the increase of soil moisture content in the slope. However, the growth rate of moisture content is different in different positions of the slope, which has the characteristic of spatial distribution. Under the action of gravity, rain water seeps downward and finally converges at the foot of the slope and flows out from

the toe of slope, so the moisture content of the soil near the foot of the slope increases the fastest and is the first to reach saturation. Whether the soil in the middle and upper part of the slope can reach saturation depends on a variety of factors, including rainfall intensity, rainfall duration, soil permeability and so on.

(3) The change of pore water pressure is directly affected by soil moisture content, so it also has the characteristics of spatial distribution. Where the water content increases rapidly, the pore water pressure also increases quickly. However, under the action of earthquake, due to the short period of earthquake action, the soil moisture content is not very sensitive to this action. The pore water pressure changes sharply during the earthquake. The peak value of pore water pressure changes almost synchronously with that of seismic load, and this is called the transient pore pressure response. On the whole, there are two responses for the pore water pressure: transient response and cumulative response. The cumulative response characteristics of pore water pressure appear in the place where obvious plastic deformation of soil occurs in the slope. When the slope soil has only elastic deformation but no obvious plastic deformation, the pore water pressure is mainly transient response.

(4) Under the combined action of rainfall and earthquake, there is a multi-physical field effect in the slope, i.e., softening effect of soil induced by rain water, increasing effect of pore water pressure and dynamic effect induced by earthquake. Rainfall weakens the strength of the soil, mainly causes local instability of the slope. More extensive damage of the slope is caused under the combined action of seismic inertia force.

Acknowledgements This work is supported by National Natural Science Foundation of China (10902112), Sichuan Provincial Science and Technology Plan Project (2021YFS0323, 2020YFG0123).

Funding The authors have not disclosed any funding.

Declarations

Conflict of interest The authors declare that they have no conflict of interest.

References

Chang KT, Chiang SH, Hsu ML (2007) Modeling typhoon- and earthquake induced landslides in a mountainous watershed using logistic regression. Geomorphology 89:335–347. https://doi.org/10.1016/j.geomorph.2006.12.011

Chang ZL, Huang FM, Huang JS, Jiang SH, Zhou CB, Zhu L (2021) Experimental study of the failure mode and mechanism of loess fill slopes induced by rainfall. Eng Geol 280:105941. https://doi.org/10.1016/j.enggeo.2020.105941

Chen ZL, Xu Q, Hu X (2013) Study on dynamic response of the 'Dualistic' structure rock slope with seismic wave theory. J Mount Sci 10(6):996–1007. https://doi.org/10.1007/s11629-012-2490-7

Chen J, Wang L, Xiaowu P, Li F, Li T (2020) Experimental study on the dynamic characteristics of low-angle loess slope under the influence of long- and short-term effects of rainfall before earthquake. Eng Geol 273(July 2019):105684. https://doi.org/10.1016/j.enggeo.2020.105684

Du XL, Lu DC (2011) Advances in soil dynamics and geotechnical earthquake engineering. Rock Soil Mech 32(S2):10–20 (**in Chinese**)

Faris F, Wang FW (2014) Investigation of the initiation mechanism of an earthquake- induced landslide during rainfall: a case study of the Tandikat Landslide, West Sumatra, Indonesia. Geoenviron Disasters 1(1):1–18. https://doi.org/10.1186/s40677-014-0004-3

Lin CW, Liu SH, Lee SY, Liu CC (2006) Impacts of the Chi-Chi earthquake on subsequent rainfall-induced landslides in central Taiwan. Eng Geol 86:87–101

Lin HC, Yu YZ, Li GX, Peng JB (2009) Influence of rainfall characteristics on soil slope failure. Chin J Rock Mech Eng 28(1):198–204
Lu XB, Ye TL, Zhang XH, Cui P, Hu KH (2012a) Experimental and numerical analysis on the responses of slope under rainfall. Nat Hazards. https://doi.org/10.1007/s11069-012-0277-3
Lu XB, Cui P, Chen XQ, Hu KH (2012b) Evolution of shear zones using numerical analysis at the May 12th Wenchuan Earthquake Site, China. Environ Earth Sci 65:1029–1036
Martino S, Antonielli B, Bozzano F, Caprari P, Discenza ME, Esposito C, Fiorucci M, Iannucci R, Marmoni GM, Schilirò L (2020) Landslides triggered after the 16 August 2018 Mw 5.1 Molise Earthquake (Italy) by a combination of intense rainfalls and seismic shaking. Landslides 17(5):1177–1190. https://doi.org/10.1007/s10346-020-01359-w
Moriwaki H, Inokuchi T, Hattanji T, Sassa K, Ochiai H, Wang G (2004) Failure processes in a full-scale landslide experiment using a rainfall simulator. Landslides 1:277–288
Song DQ, Liu XL, Huang J, Zhang YF, Zhang JM (2021) Seismic cumulative failure effects on a reservoir bank slope with a complex geological structure considering plastic deformation characteristics using shaking table tests. Eng Geol 286:106085. https://doi.org/10.1016/j.enggeo.2021.106085
Srilatha N, Latha GM, Puttappa CG (2013) Effect of frequency on seismic response of reinforced soil slopes in shaking table test. Geotext Geomembr 36:27–32
Taylor DW (1937) Stability of earth slopes. J Bost Soc Civ Eng 24:197–246
Tohari A, Nishigaki M, Komatsu M (2007) Laboratory rainfall-induced slope failure with moisture content measurement. J Geotech Geoenviron Eng 133(5):575–587
Wang G, Sassa K (2003) Pore pressure generation and movement of rainfall- induced landslides: effects of grain size and fine particle content. Eng Geol 69:109–125
Wang LM, Wang Q, Wu ZJ, et al (2017a) Loessial landslides induced by the Minxian–Zhangxian Ms6.6 earthquake of China in 2013. In: Geotechnical hazards from large earthquakes and heavy rainfalls. Springer, Japan. https://doi.org/10.1007/978-4-431-56205-4_17
Wang J, Zhang D, Wang N, Gu T (2019) Mechanisms of wetting-induced loess slope failures. Landslides 16(5):937–953. https://doi.org/10.1007/s10346-019-01144-4
Wang Q, Wang Z, Su Y et al (2021) Characteristics and mechanism of the landslide in Yongguang village, Minxian County, China. Nat Hazards 105:1413–1438. https://doi.org/10.1007/s11069-020-04360-7
Wartman J, Raymond BS, Jonathan DB (2005) Shaking table modeling of seismically induced deformations in slopes. J Geotech Geoenviron Eng 131(5):610–622
Wu LZ, Zhou Y, Sun P, Shi JS, Liu GG, Bai LY (2017) Laboratory characterization of rainfall-induced loess slope failure. CATENA 150:1–8
Yang T, Man-chu RY, Yang B, Liu YJ, Yang YX (2016) Three-dimensional stability of landslides based on local safety factor. J Mt Sci 13(9):1515–1526
Yang B, Gao FP, Jeng DS (2018) Failure mode and dynamic response of a double-sided slope with high water content of soil. J Mt Sci 15(4):859–870
Yang B, Luo Y, Jeng DS, Feng J (2019) Effects of moisture content on the dynamic response and failure mode of unsaturated soil slope subjected to seismic load. Bull Seismol Soc Am 109(2):489–504. https://doi.org/10.1785/0120180222
Zhang LL, Zhang J, Zhang LM, Tang WH (2011) Stability analysis of rainfall-induced slope failure: a review. Proc Inst Civ Eng Geotech Eng 164(5):299–316